Chemical Science

ROYAL SOCIETY OF CHEMISTRY

EDGE ARTICLE

View Article Online
View Journal

Cite this: DOI: 10.1039/d6sc02144a

All publication charges for this article have been paid for by the Royal Society of Chemistry

Quinoid-controlled bond-length alternation enables high-mobility non-fused π-conjugated polymers

Tsubasa Mikie, *[ab] Keitaro Iguchi,[a] Ryosuke Kamimura,[b] Kenta Tanaka,[a] Hiroyuki Ishii [cd] and Itaru Osaka *[ab]

Received 15th March 2026
Accepted 1st June 2026

DOI: 10.1039/d6sc02144a

rsc.li/chemical-science

Achieving high charge-carrier mobility in π-conjugated polymers typically requires the incorporation of fused-ring frameworks that ensure backbone planarity and rigidity (intrachain transport) and π–π stacking (interchain transport). Here we show that high mobility can instead arise from efficient intrachain transport even in fully non-fused polymer backbones through precise control of quinoid resonance and bond-length alternation (BLA). A series of S-Pechmann (SP)-based polymers having alkoxy side chains were designed in which the quinoidal character was systematically tuned by varying the length of the oligothiophene co-units. Increasing quinoidal character markedly suppresses BLA along the polymer backbone, leading to pronounced π-electron delocalization and reduced carrier effective masses as low as $\sim 0.05 m_0$ in theory. As a result, the polymers exhibit ambipolar organic field-effect transistor (OFET) characteristics with mobilities of up to 4.4 $cm^2 V^{-1} s^{-1}$ for holes and 3.4 $cm^2 V^{-1} s^{-1}$ for electrons, despite moderate crystallinity and a predominantly face-on orientation that is typically unfavorable for OFET operation. These findings reveal how quinoid-induced modulation of BLA governs intrachain charge transport in conjugated polymers and highlight BLA modulation as a promising molecular design strategy for achieving high mobility in π-conjugated polymers beyond the conventional fused-ring approach.

Introduction

Charge transport in π-conjugated polymers is a fundamental property that determines their performance in organic electronic devices.[1–3] In many high-mobility π-conjugated polymers, charge transport has traditionally been improved by enhancing intermolecular π–π stacking and crystallinity, which facilitate interchain charge transport.[4,5] More recently, however, efficient intrachain charge transport through a continuous π-orbital network has been recognized as an increasingly important factor governing the mobility of π-conjugated polymers.[6,7] In this context, promoting π-electron delocalization along the polymer backbone has emerged as an important molecular design strategy for improving intrachain transport.

One strategy to enhance π-electron delocalization is to increase backbone rigidity and coplanarity in order to suppress conformational disorder along the polymer backbone.[8] This approach relies primarily on the design of backbone geometry, typically through the incorporation of extended fused aromatic frameworks, as exemplified by polymer systems such as poly(indacenodithiophene-*alt*-benzothiadiazole) (pIDTBT).[9,10] In contrast, an alternative strategy to enhance π-electron delocalization is to modulate the electronic structure of the conjugated backbone by reducing bond-length alternation (BLA), which can be achieved by increasing the quinoidal character of the backbone.[11,12] Because BLA directly influences the electronic band structure of conjugated backbones, its suppression can reduce carrier effective mass and thereby promote efficient intrachain charge transport.

We recently reported a series of thienoquinoid-based polymers terminated with ketone groups,[13,14] which significantly reduce BLA along the backbone. In particular, an S-Pechmann (SP)-based polymer, **PSP4T** (Fig. 1), exhibits small BLA despite its backbone consisting entirely of non-fused rings, leading to low carrier effective masses along the backbone and high charge-carrier mobilities of ~ 2.5 $cm^2 V^{-1} s^{-1}$ in organic field-effect transistor (OFET) devices.[15] However, the fundamental relationship between quinoidal character, BLA, carrier effective mass, and charge transport in π-conjugated polymers remains largely unexplored.

[a]*Graduate School of Advanced Science and Engineering, Hiroshima University, 1-4-1 Kagamiyama, Higashi-Hiroshima, Hiroshima 739-8527, Japan. E-mail: mikie@hiroshima-u.ac.jp; iosaka@hiroshima-u.ac.jp*

[b]*School of Engineering, Hiroshima University, 1-4-1 Kagamiyama, Higashi-Hiroshima, Hiroshima 739-8527, Japan*

[c]*Institute of Pure and Applied Sciences, University of Tsukuba, Tsukuba, Ibaraki 305-8573, Japan*

[d]*Research Center for Organic–Inorganic Quantum Spin Science and Technology (OIQSST), University of Tsukuba, Tsukuba, Ibaraki 305-8573, Japan*

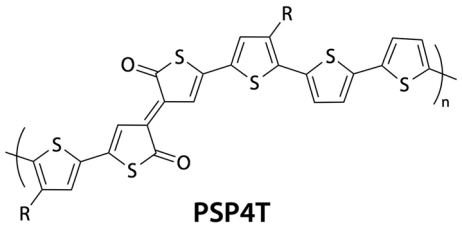

Fig. 1 Chemical structure of an S-Pechmann (SP)-based polymer, PSP4T.

In this work, we address this question by designing a series of SP-based polymers, in which the degree of quinoidal character is systematically tuned through variation of oligothiophene units. This molecular design allows us to modulate BLA along the polymer backbone and examine its impact on carrier effective mass, π-electron delocalization, and charge transport properties. In addition, we attached alkoxy groups as the side chains, rather than alkyl groups, as it induces intramolecular S···O non-covalent interactions between the sulfur atom of the SP moiety and the oxygen atom of the alkoxy substituent. These interactions suppress backbone torsion and promote a more coplanar structure, thereby further enhancing π-electron delocalization along the backbone (Fig. 2).[16] As a result, these polymers exhibit ambipolar OFET characteristics, with hole and electron mobilities exceeding 4 $cm^2 V^{-1} s^{-1}$ and 3 $cm^2 V^{-1} s^{-1}$, respectively.

Polymer synthesis

Scheme 1 illustrates the synthetic route to the SP-based polymers. The 2-decyltetradecyl group was employed as the alkyl moiety of the alkoxy side chain to ensure sufficient solubility. 5,5′-Dibromo-3,3′-bithiophene (**1**) was first coupled with 5-trimethylsilyl-2-stannyl-3-alkoxythiophene (**2**) to afford **3**. Through sequential lithiation with *n*-butyl lithium (*n*-BuLi), borylation with 2-methoxy-4,4,5,5-tetramethyl-1,3,2-dioxaborolane (MeOBpin), and oxidation with oxone, **3** was converted into an SP derivative (**4**), which was subsequently dibrominated to yield the SP-based monomer (**5**). The polymers **PSPa4T**, **PSPa3T**, and **PSPa2T** were then synthesized *via* the Migita–Kosugi–Stille polycondensation of **5** with 5,5′-bis(trimehylstannyl)-2,2′-bithiophene, 2,5-bis(trimethylstannyl) thiophene, and hexamethyldithin, respectively, using $Pd(PPh_3)_4$ as the catalyst. The number-average and weight-average molecular weights (M_n and M_w) were 24 000 and 53 100 for **PSPa4T**, 18 700 and 29 900 for **PSPa3T**, and 12 800 and 24 300 for **PSPa2T**, respectively (Fig. S1 and Table S1). **PSPa4T** was soluble in hot *o*-dichlorobenzene and **PSPa3T** and **PSPa2T** were soluble in hot chloroform and chlorobenzene. Differential scanning calorimetry (DSC) confirmed that all polymers exhibited thermal stability up to at least 300 °C, indicative of robust polymer structures (Fig. S2).

Polymer properties

The energy levels of the SP-based polymers were evaluated by cyclic voltammetry, and the relevant parameters are summarized in the energy diagram (Fig. 3a and b). The highest occupied molecular orbital (HOMO) and lowest unoccupied molecular orbital (LUMO) energy levels (E_{HOMO} and E_{LUMO}) were determined based on the onset potentials of oxidation and reduction peaks in the cyclic voltammograms (Fig. 3a). The E_{LUMO} values progressively downshifted with decreasing the number of thiophene rings in the repeating unit, while the E_{HOMO} values remained similar around −5.0 eV. Specifically, the E_{HOMO}/E_{LUMO} values were −4.98/−3.72 eV for **PSPa4T**, −4.99/−3.81 eV for **PSPa3T**, and −5.00/−3.94 eV for **PSPa2T** (Fig. 3b). These E_{HOMO} values are higher than those of **PSP4T** by 0.25 eV, which is due to the electron-donating nature of the alkoxy group. A similar trend in E_{HOMO} values for each polymer was also confirmed by photoelectron yield spectroscopy (PYS) measurements (Fig. S3). These experimental energy levels are in good agreement with the DFT results calculated at the B3LYP 6-31G(d) level of theory (Fig. S4).

The UV-vis-NIR absorption spectra of the polymers in the thin films are shown in Fig. 3c and the corresponding optical parameters are summarized in Table 1. **PSPa4T** exhibited an absorption spectrum with a maximum (λ_{max}) and onset (λ_{onset}) at around 1107 nm and 1466 nm, respectively, which were slightly red-shifted to 1112 nm and 1580 nm in **PSPa3T**, respectively. The optical bandgap (E_g^{opt}) estimated from the Tauc plot was 0.82 eV for **PSPa4T** and 0.73 eV for **PSPa3T** (Fig. S5). Notably, **PSPa2T** displayed a more pronounced red-shifted absorption band with $\lambda_{max}/\lambda_{edge}$ values of 1413/2170 nm. Such an exceptionally long-wavelength absorption has rarely been observed in non-fused π-conjugated polymers. This remarkable bathochromic shift corresponds to an ultranarrow E_g^{opt} of

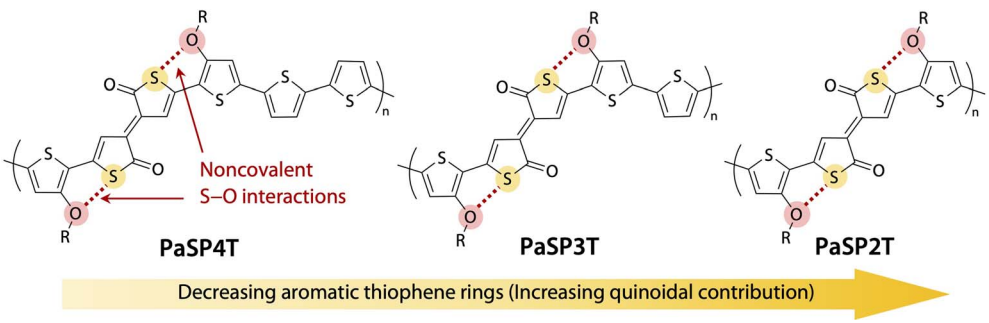

Fig. 2 Chemical structures of SP-based polymers bearing alkoxy groups (PSPa4T, PSPa3T, and PSPa2T).

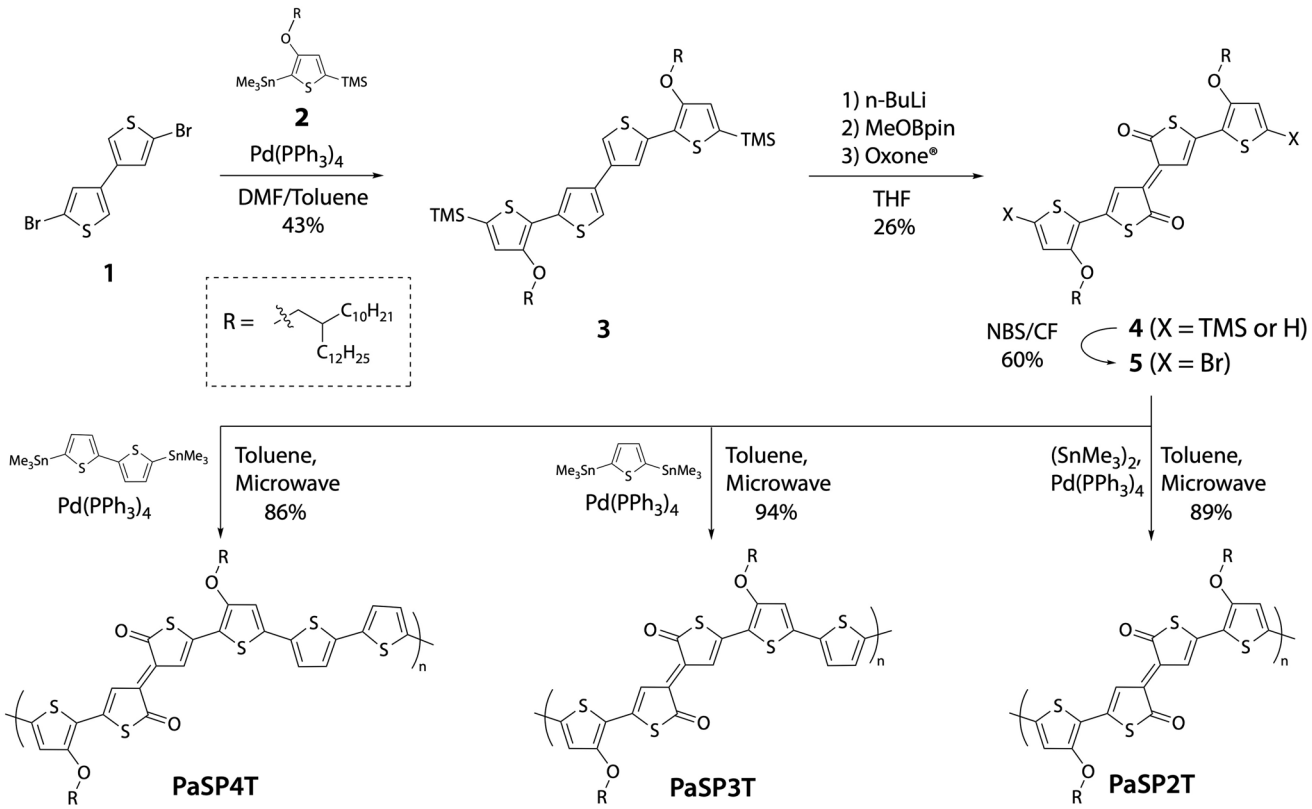

Scheme 1 Synthetic route for the SP-based polymers.

0.56 eV, placing **PSPa2T** among the lowest-gap polymers reported to date.[17–19] Because **PSPa2T** exhibits strong absorption in the SWIR region but minimal absorption in the visible region, both its solution and film appear nearly transparent (Fig. S6).

To elucidate how the number of aromatic thiophene rings influences the quinoidal character of the polymer backbone, we compared the C–C and C=C bond lengths extracted from the central repeat units of optimized model trimers using DFT calculations. In all cases, the backbone appeared mostly coplanar originating from the S···O interaction between the SP moiety and alkoxythiophene. Fig. 4a–c show the chemical structures and corresponding C–C and C=C bond lengths of **PSPa4T**, **PSPa3T**, and **PSPa2T**, respectively. For the SP core (shown in blue), the length of the C–C bond (bond numbers 5, 7, 9, and 11) and the C=C bond (bond numbers 6, 8, and 10) became shorter and longer, respectively, as the number of thiophene rings in the repeating unit decreased, *i.e.*, upon going from **PSPa4T** to **PSPa3T** and then to **PSPa2T**, indicating the enhancement of quinoidal character in this order. Similarly, for the alkoxythiophenes (shown in red), the length of the C–C bond (bond numbers 1, 3, 13, and 15) and C=C bond (bond numbers 2, 4, 12, and 14) becomes shorter and longer, respectively, in the same order. In addition, the C–C and C=C bonds

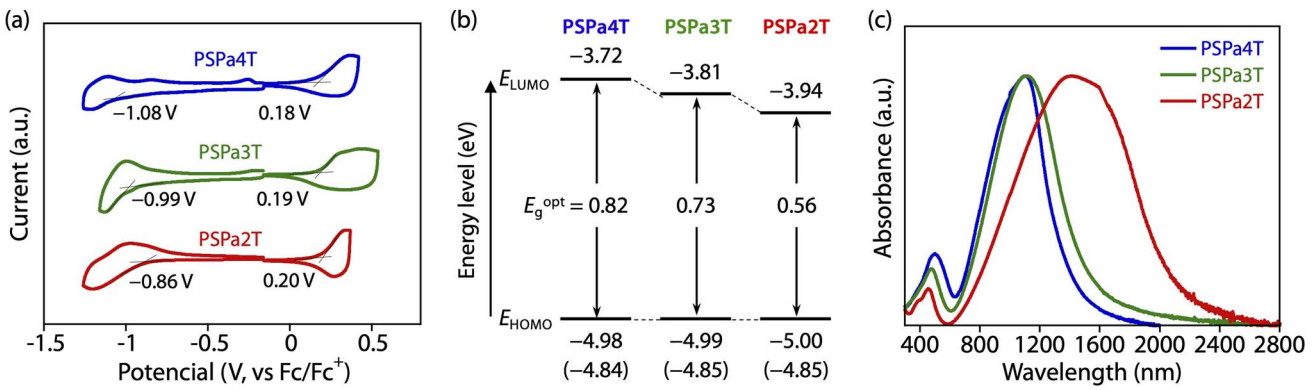

Fig. 3 (a) Cyclic voltammogram, (b) energy diagram, and (c) UV-vis-NIR absorption spectra of the polymers.

Table 1 Optical parameters and calculated effective mass of SP-based polymers

Polymer	λ_{max} (nm)	λ_{onset} (nm)	E_g^{opt} (eV)	m_h[a] (m_0)	m_e[a] (m_0)
PSPa4T	1107	1466	0.82	0.096	0.095
PSPa3T	1112	1580	0.73	0.072	0.077
PSPa2T	1413	2170	0.56	0.051	0.049

[a] Effective masses for hole (m_h) and electron (m_e).

for unsubstituted thiophenes (shown in grey) were shorter and longer, respectively, in **PSPa3T** than in **PSPa4T**. The result clearly shows that bond length alternation (BLA) became smaller with a decreasing number of aromatic thiophene units in the repeating unit, explaining the decrease in E_g. Notably, BLA was significantly reduced when the unsubstituted thiophene was absent (**PSPa2T**). The result is consistent with the "dilution effect" reported for *para*-azaquinodimethane-based polymers.[20]

With the decreased BLA due to the decreased number of aromatic thiophene rings, an increase in intrachain transport is expected. We therefore conducted band-structure calculations based on density functional theory using the plane-wave basis set (Fig. 4d–f).[21,22] The polymer structures are obtained as follows. First, we optimized the molecular structure of the trimer of the repeat unit for each polymer, where the alkoxy groups were replaced with the methoxy group, using quantum chemical calculations at the B3LYP/6-31G(d) level. Then we obtained the electronic band structures for the polymer structures with the periodic boundary condition using the central repeat unit in the trimer model. Generally gradient approximation was employed to obtain the exchange–correlation functionals. The cutoff energies for the plane wave and charge density are 60 and 400 Ry, and the Brillouin zone integration is performed with an $8 \times 2 \times 2$ k-point set. Upon going from **PSPa4T** to **PSPa3T**, and to **PSPa2T**, the HOMO and LUMO were up-shifted and down-shifted, respectively, reducing the bandgap; the theoretical bandgap was found to be 0.44, 0.34, and 0.17 eV for **PSPa4T**, **PSPa3T**, and **PSPa2T**, respectively. We then estimated the effective masses of holes (m_h) and electrons (m_e) along the polymer backbone according to the acoustic deformation potential model (Table 1). For **PSPa4T**, m_h and m_e

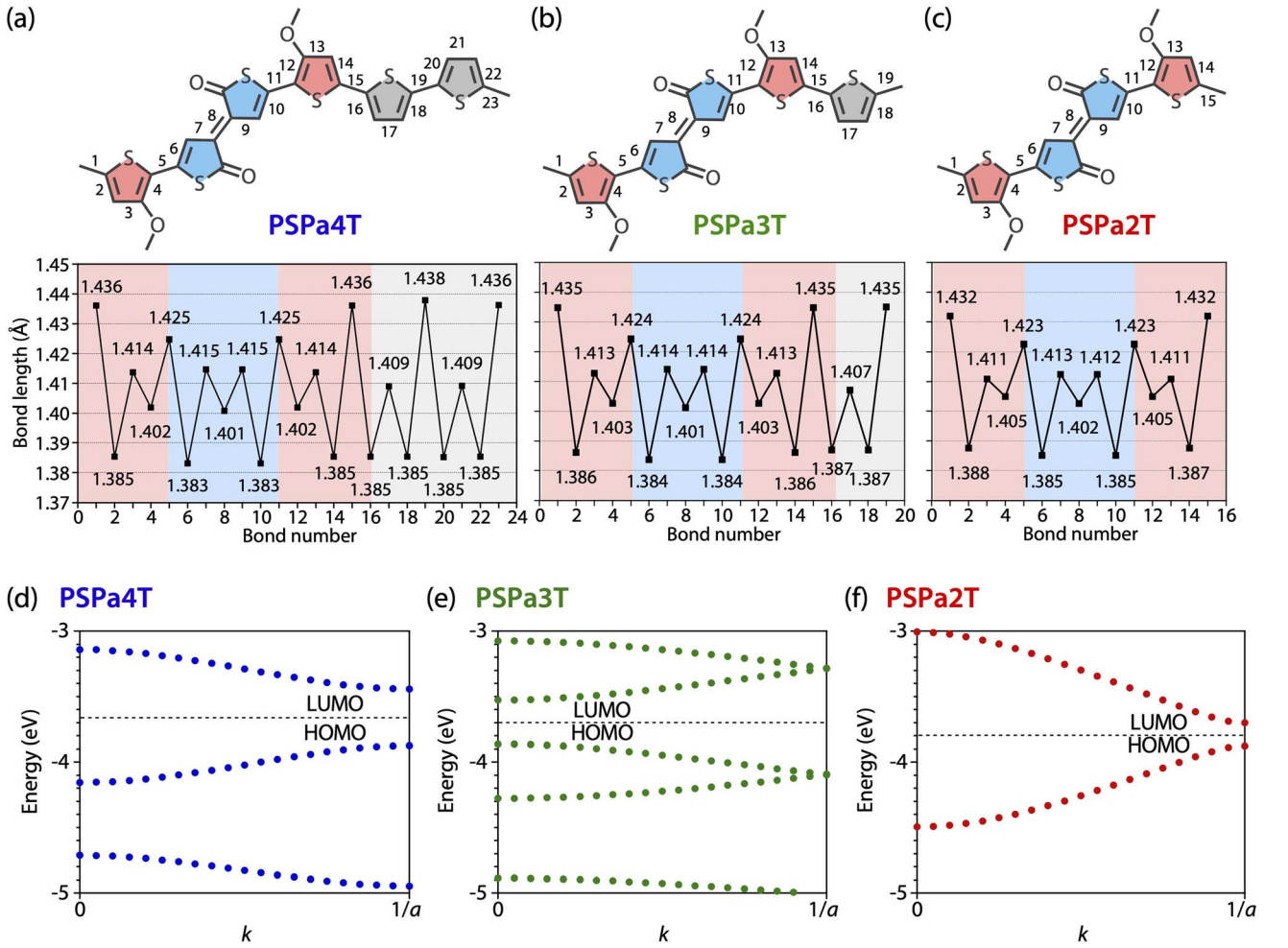

Fig. 4 (a–c) Plots of the lengths of carbon–carbon single bonds (bonds in even numbers) and double bonds (bonds in odd numbers) at the respective bond number shown in (a) **PSPa4T**, (b) **PSPa3T**, and (c) **PSPa2T**. (d–f) Band structure of (d) **PSPa4T**, (e) **PSPa3T**, and (f) **PSPa2T**. The broken line represents the Fermi energy.

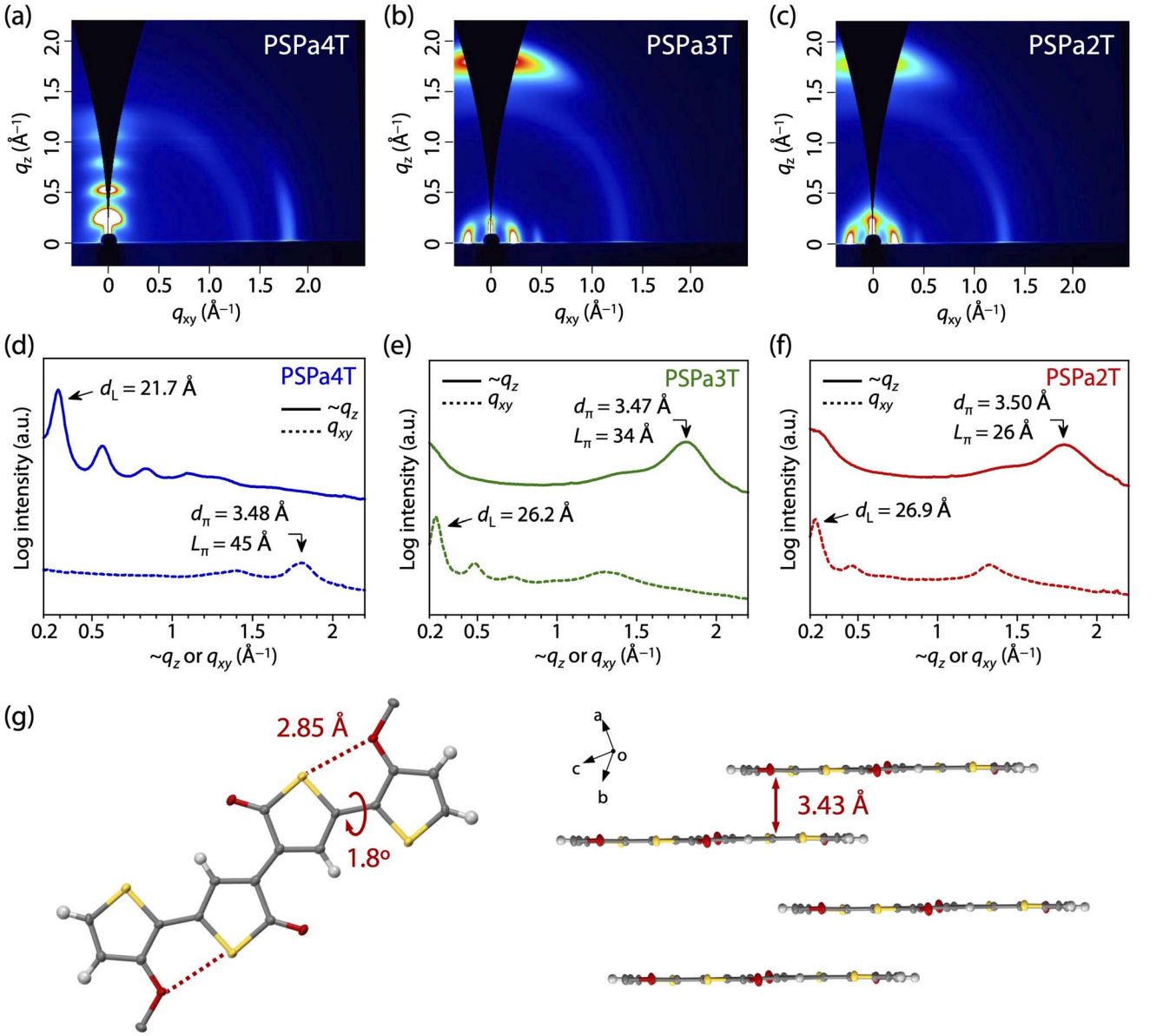

Fig. 5 (a–c) 2D GIXD patterns of polymer thin films. (d–f) Cross-sectional diffraction profiles cut from the 2D GIXD patterns along quasi-q_z and q_{xy} axes. (g) Molecular structure of model compound **SPa2T** determined by single-crystal X-ray analysis (CCDC Deposition Number 2518599). Only the methyloxy moieties are shown as the hexyloxy groups in **SPa2T** at the β-position of the thiophene ring for clarity.

were $0.096m_0$ and $0.095m_0$, respectively, where m_0 is the electron rest mass. These values were higher than those of **PSP4T** (m_h/m_e = $0.068/0.076m_0$), *i.e.*, charge transport is lower.[20] This is ascribed to the position of the side chain, which alters the bond length (Fig. S7). In fact, **PSPi4T**, in which the alkyl group is on the neighboring carbon in **PSP4T**, also had higher m_h and m_e values of $0.099m_0$ and $0.12m_0$, respectively (Fig. S8 and Table S2). For **PSPa3T** and **PSPa2T**, both m_h and m_e decreased in this order, *i.e.*, as the number of thiophene rings in the repeat unit decreased: $0.0722/0.0771m_0$ for **PSPa3T**, and $0.0506/0.0490m_0$ for **PSPa2T**. The effective mass for **PSPa3T** and **PSPa2T** is even lower than that for pIDTBT ($0.097m_0$), one of the fused-ring π-conjugated polymers considered to have high intramolecular charge transport, confirming that, in theory, significantly high charge delocalization and thereby charge transport can be realized within the non-fused backbone. Taken together, reducing BLA *via* quinoidal resonance effectively decreases the effective mass.

Thin film structure

We investigated the molecular ordering and orientation of polymer thin films using grazing incidence X-ray diffraction (GIXD) (Fig. 5). **PSPa4T** exhibited pronounced π–π stacking and lamellar diffraction peaks along the q_{xy} and q_z axes, respectively, indicative of a predominant edge-on orientation that is favorable for in-plane charge transport and thus for OFETs (Fig. 5a and d). In contrast, **PSPa3T** and **PSPa2T** displayed π–π stacking

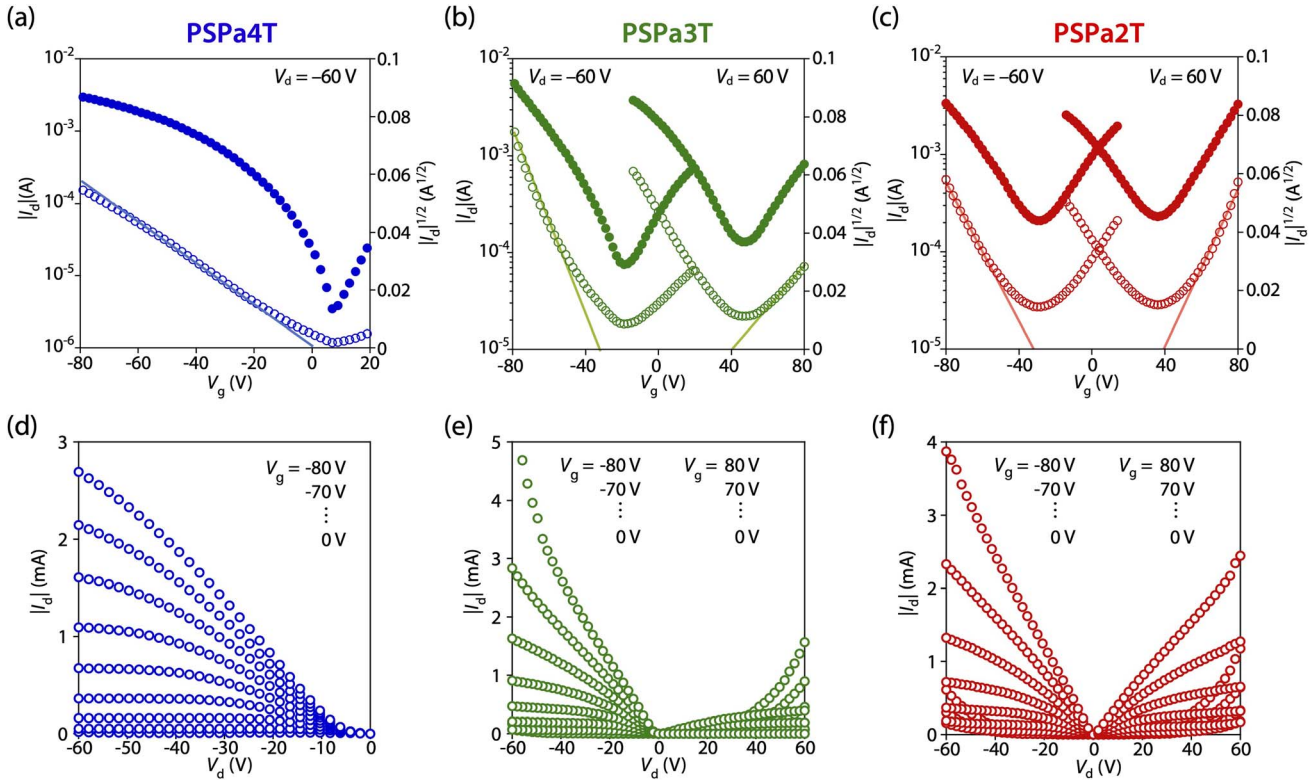

Fig. 6 (a–c) Transfer and (d–f) output curves of OFET devices: (a and d) **PSPa4T**; (b and e) **PSPa3T**; (c and f) **PSPa2T**.

Table 2 OFET characteristics

	p-channel operation		n-channel operation		
Polymer	μ_h[a] ($cm^2\ V^{-1}\ s^{-1}$)	V_{th}[b] (V)	μ_e[a] ($cm^2\ V^{-1}\ s^{-1}$)	V_{th}[b] (V)	μ_e/μ_h[c]
PSPa4T	0.98 [0.88]	0	—	—	—
PSPa3T	4.41 [2.86]	−32	0.62 [0.50]	40	0.14
PSPa2T	2.06 [1.31]	−32	3.38 [1.75]	39	1.64

[a] μ_h and μ_e denote the maximum hole and electron field-effect mobilities, respectively. The average mobilities of the top five devices are given in parentheses. [b] Threshold voltage. [c] Ratio of electron to hole mobilities.

diffraction along the q_z axis and lamellar diffraction along the q_{xy} axis, respectively, assigned to a predominant face-on orientation that typically favors out-of-plane charge transport (Fig. 5b, c, e and f). Despite these distinct backbone orientations, all polymers exhibited clear crystalline characteristics, likely arising from the high coplanarity of the polymer backbone facilitated by intramolecular noncovalent S···O interactions. The planarity of the alkoxythiophene-flanked SP core was also confirmed by the single-crystal X-ray analysis of the model compound (Fig. 5g), in which the dihedral angle between the SP core and the alkoxythiophene was only 1.8°, as well as through computation (Fig. S4). Furthermore, in the single crystal, the distance between the sulfur atom of the SP core and the oxygen atom of the alkoxythiophene was 2.86 Å, which was shorter than the sum of their van der Waals radii (3.25 Å), indicating the existence of a noncovalent interaction.

The π–π stacking distance (d_π) was comparable among the three polymers—3.48 Å for **PSPa4T**, 3.47 Å for **PSPa3T**, and 3.50 Å for **PSPa2T**—corresponding to a tight π–π stacking motif in all cases. Scherrer analysis revealed that the crystallite coherence length for the π–π stacking structure (L_π) was 45 Å for **PSPa4T**, 34 Å for **PSPa3T**, and 26 Å **for PSPa2T**. Although we note that a direct comparison of d_π and L_π values extracted from the out-of-plane and in-plane diffraction peaks is not strictly accurate, these results nevertheless suggest a trend of decreasing π–π stacking crystallinity in the order **PSPa4T** > **PSPa3T** > **PSPa2T**. This tendency is probably due to the lower molecular weight the polymers in the same order. Nevertheless, all polymers maintain short π–π stacking distances and appreciable crystallinity in thin films, which likely contributes to their high charge transport performance.

Charge transport properties

We evaluated the charge carrier transport characteristics of the SP-based polymers in OFET devices with a top-gate/bottom-contact architecture. We employed 1-octanethiol as the self-assembled monolayer for Au electrodes because alkanethiols are known to lower the work function of Au, thereby facilitating electron injection and enhancing n-channel characteristics.[23] Transfer and output curves of the devices are shown in Fig. 6a–f, respectively, and the corresponding OFET parameters are summarized in Table 2. **PSPa4T** exhibited unipolar p-type

behavior, whereas **PSPa3T** and **PSPa2T** displayed clear ambipolar behavior, as evidenced by *V*-shaped transfer curves in the saturation regime (source–drain voltage V_d of ±60 V) under both p- and n-channel operation. This trend is consistent with the downshifted E_{LUMO} values.

With respect to hole transport, **PSPa4T** exhibited a moderate hole mobility (μ_h) of up to 0.98 $cm^2 V^{-1} s^{-1}$. In sharp contrast, **PSPa3T** and **PSPa2T** showed markedly enhanced hole transport, with μ_h values of 4.41 and 2.06 $cm^2 V^{-1} s^{-1}$, respectively. To the best of our knowledge, the μ_h of 4.41 $cm^2 V^{-1} s^{-1}$ achieved by **PSPa3T** is among the highest hole mobilities reported for π-conjugated polymers with fully non-fused backbones. Remarkably, **PSPa3T** and **PSPa2T** outperformed **PSPa4T** despite their face-on backbone orientation, which is typically unfavorable for in-plane charge transport. This trend strongly suggests that the charge carrier mobility in this series is governed primarily by intrachain transport rather than interchain transport. This is further supported by the significantly smaller effective mass calculated along the backbone as discussed above. The slightly lower μ_h in **PSPa2T** than in **PSPa3T** may be due to its increased n-channel character (decreased p-channel character) as described below. Regarding electron transport, in fact, **PSPa3T** and **PSPa2T** exhibited distinct n-channel characteristics with μ_e values of 0.62 and 3.38 $cm^2 V^{-1} s^{-1}$, respectively, while **PSPa4T** showed no appreciable n-channel behavior. Therefore, decreasing the number of thiophene rings clearly enhances the n-channel characteristics, reflected in the electron-to-hole mobility ratio (μ_e/μ_h) of 0.14 for **PSPa3T** and 1.64 for **PSPa2T**. The μ_e of 3.38 $cm^2 V^{-1} s^{-1}$ for **PSPa2T** is likewise among the highest values reported for π-conjugated polymers with fully non-fused backbones, underscoring the remarkable n-type capability enabled by the quinoid-rich architecture.

Overall, increasing the quinoidal character by reducing the number of thiophene rings in the repeat unit substantially improves charge carrier transport, achieving mobilities in excess of 4 $cm^2 V^{-1} s^{-1}$ for holes and 3 $cm^2 V^{-1} s^{-1}$ for electrons, primarily by promoting intrachain charge transport while simultaneously strengthening n-channel characteristics. While a reduction in thiophene ring number is known to enhance quinoidal character, previous reports have not identified a clear relationship between increased quinoidal character, *i.e.*, BLA, and charge carrier mobility.[20,24] By contrast, in this SP-based system, reduced BLA achieved through shortening the oligothiophene unit is directly reflected in higher mobility, highlighting the crucial role of BLA in intrachain charge delocalization and charge transport.

Conclusions

In summary, we have demonstrated that high charge transport can be achieved in fully non-fused π-conjugated backbones through careful design of quinoidal character and BLA. By incorporating an SP quinoid core flanked by alkoxythiophene units and systematically tuning the length of the oligothiophene co-unit, we modulated the quinoidal character and BLA along the polymer backbone while promoting backbone coplanarity through intramolecular non-covalent interactions. This design resulted in strong intrachain π-electron delocalization as evidenced by reduced carrier effective mass as low as $\sim 0.05 m_0$, enabling p-type to ambipolar characteristics with mobilities as high as 4.4 $cm^2 V^{-1} s^{-1}$ for holes and 3.4 $cm^2 V^{-1} s^{-1}$ for electrons, the highest level for fully non-fused systems. Despite their moderate crystallinity and predominantly face-on orientation, these polymers exhibit high charge-carrier mobilities, indicating that charge transport in this series is governed primarily by efficient intrachain processes rather than π–π stacking. These findings highlight the importance of controlling BLA as an electronic-structure design parameter for promoting intrachain charge transport. The concept demonstrated here opens new possibilities for developing structurally simple and high-mobility π-conjugated polymers for next-generation organic electronics.

Author contributions

K. I. and R. K. synthesized the polymers and carried out the OFET experiments. K. I. synthesized the model compounds, CV, UV-vis, and 2D GIXD measurements. K. T. supported the synthesis of the intermediate compounds. H. I. calculated the band structures and effective masses. T. M. and I. O. prepared the manuscript, and all authors discussed and commented on the manuscript. T. M. and I. O. directed the project.

Conflicts of interest

There are no conflicts to declare.

Data availability

CCDC 2518599 contains the supplementary crystallographic data for this paper.[25]

The data supporting this article have been included as part of the supplementary information (SI). Supplementary information is available. See DOI: https://doi.org/10.1039/d6sc02144a.

Acknowledgements

This research was supported by Grants-in-Aid for Scientific Research from Japan Society for the Promotion of Science (Grant No. 22K14745) and CREST from Japan Science and Technology Agency (Grant No. JPMJCR21Q1). 2D GIXD experiments were performed at SPring-8 with the approval of the Japan Synchrotron Radiation Research Institute (Proposal No. 2025A1652). We thank Dr Tomoyuki Koganezawa for his support with 2D GIXD experiments.

References

1 S. Fratini, M. Nikolka, A. Salleo, G. Schweicher and H. Sirringhaus, *Nat. Mater.*, 2020, **19**, 491–502.
2 L. Luo, W. Huang, C. Yang, J. Zhang and Q. Zhang, *Front. Phys.*, 2021, **16**, 33500.

3 A. Chougle, A. Rezk, S. U. B. Afzal, A. K. Mohammed, D. Shetty and A. Nayfeh, *Nano-Micro Lett.*, 2025, **17**, 230.
4 H. Sirringhaus, P. J. Brown, R. H. Friend, M. M. Nielsen, K. Bechgaard, B. M. W. Langeveld-Voss, A. J. H. Spiering, R. A. J. Janssen, E. W. Meijer, P. Herwig and D. M. de Leeuw, *Nature*, 1999, **401**, 685–688.
5 H. N. Tsao, D. M. Cho, I. Park, M. R. Hansen, A. Mavrinskiy, D. Y. Yoon, R. Graf, W. Pisula, H. W. Spiess and K. Müllen, *J. Am. Chem. Soc.*, 2011, **133**, 2605–2612.
6 X. Zhang, H. Bronstein, A. J. Kronemeijer, J. Smith, Y. Kim, R. J. Kline, L. J. Richter, T. D. Anthopoulos, H. Sirringhaus, K. Song, M. Heeney, W. Zhang, I. McCulloch and D. M. DeLongchamp, *Nat. Commun.*, 2013, **4**, 2238.
7 G. LeCroy, R. Ghosh, P. Sommerville, C. Burke, H. Makki, K. Rozylowicz, C. Cheng, M. Weber, W. Khelifi, N. Stingelin, A. Troisi, C. Luscombe, F. C. Spano and A. Salleo, *J. Am. Chem. Soc.*, 2024, **146**, 21778–21790.
8 D. Venkateshvaran, M. Nikolka, A. Sadhanala, V. Lemaur, M. Zelazny, M. Kepa, M. Hurhangee, A. J. Kronemeijer, V. Pecunia, I. Nasrallah, I. Romanov, K. Broch, I. McCulloch, D. Emin, Y. Olivier, J. Cornil, D. Beljonne and H. Sirringhaus, *Nature*, 2014, **515**, 384–388.
9 W. Zhang, J. Smith, S. E. Watkins, R. Gysel, M. McGehee, A. Salleo, J. Kirkpatrick, S. Ashraf, T. Anthopoulos, M. Heeney and I. McCulloch, *J. Am. Chem. Soc.*, 2010, **132**, 11437–11439.
10 A. Wadsworth, H. Chen, K. J. Thorley, C. Cendra, M. Nikolka, H. Bristow, M. Moser, A. Salleo, T. D. Anthopoulos, H. Sirringhaus and I. McCulloch, *J. Am. Chem. Soc.*, 2019, **142**, 652–664.
11 J. L. Brédas, *J. Chem. Phys.*, 1998, **82**, 3808–3811.
12 I. Hoogmartens, P. Adriaensens, D. Vanderzande, J. Gelan, C. Quattrocchi, R. Lazzaroni and J. L. Brédas, *Macromolecules*, 1992, **25**, 7347–7356.
13 I. Osaka, T. Abe, H. Mori, M. Saito, N. Takemura, T. Koganezawa and K. Takimiya, *J. Mater. Chem. C*, 2014, **2**, 2307–2312.
14 K. Kawabata, M. Saito, I. Osaka and K. Takimiya, *J. Am. Chem. Soc.*, 2016, **138**, 7725–7732.
15 T. Mikie, M. Hayakawa, K. Okamoto, K. Iguchi, S. Yashiro, T. Koganezawa, M. Sumiya, H. Ishii, S. Yamaguchi, A. Fukazawa and I. Osaka, *Chem. Mater.*, 2021, **33**, 8183–8193.
16 H. Huang, L. Yang, A. Facchetti and T. J. Marks, *Chem. Rev.*, 2017, **117**, 10291–10318.
17 J. Fan, J. D. Yuen, M. Wang, J. Seifter, J. H. Seo, A. R. Mohebbi, D. Zakhidov, A. Heeger and F. Wudl, *Adv. Mater.*, 2012, **24**, 2186–2190.
18 T. T. Steckler, P. Henriksson, S. Mollinger, A. Lundin, A. Salleo and M. R. Andersson, *J. Am. Chem. Soc.*, 2014, **136**, 1190–1193.
19 H. Cai, H. Tang, T. Wang, C. Xu, J. Xie, M. Fu, X. Luo, Z. Hu, Y. Zhang, Y. Deng, G. Li, C. Liu, F. Huang and Y. Cao, *Angew. Chem., Int. Ed.*, 2024, **63**, e202402375.
20 X. Liu, B. He, C. L. Anderson, J. Kang, T. Chen, J. Chen, S. Feng, L. Zhang, M. A. Kolaczkowski, S. J. Teat, M. A. Brady, C. Zhu, L.-W. Wang, J. Chen and Y. Liu, *J. Am. Chem. Soc.*, 2017, **139**, 8355–8363.
21 J. E. Northrup, *Phys. Rev. B: Condens. Matter Mater. Phys.*, 2007, **76**, 245202.
22 P. Giannozzi, S. Baroni, N. Bonini, M. Calandra, R. Car, C. Cavazzoni, D. Ceresoli, G. L. Chiarotti, M. Cococcioni, I. Dabo, A. D. Corso, S. de Gironcoli, S. Fabris, G. Fratesi, R. Gebauer, U. Gerstmann, C. Gougoussis, A. Kokalj, M. Lazzeri, L. Martin-Samos, N. Marzari, F. Mauri, R. Mazzarello, S. Paolini, A. Pasquarello, L. Paulatto, C. Sbraccia, S. Scandolo, G. Sclauzero, A. P. Seitsonen, A. Smogunov, P. Umari and R. M. Wentzcovitch, *J. Phys.: Condens. Matter*, 2009, **21**, 395502.
23 D. Boudinet, M. Benwadih, Y. Qi, S. Altazin, J.-M. Verilhac, M. Kroger, C. Serbutoviez, R. Gwoziecki, R. Coppard, G. L. Blevennec, A. Kahn and G. Horowitz, *Org. Electron.*, 2010, **11**, 227–237.
24 K. F. Cheng, C.-L. Liu and W.-C. Chen, *J. Polym. Sci., Part A:Polym. Chem.*, 2007, **45**, 5872–5883.
25 CCDC 2518599: Experimental Crystal Structure Determination, 2026, DOI: 10.5517/ccdc.csd.cc2qjt47.